



## Green electrospun pantothenic acid/silk fibroin composite nanofibers: Fabrication, characterization and biological activity



Linpeng Fan<sup>a,b,c</sup>, Zengxiao Cai<sup>b,c</sup>, Kuihua Zhang<sup>a,b</sup>, Feng Han<sup>b</sup>, Jingliang Li<sup>c</sup>, Chuanglong He<sup>a,b</sup>, Xiumei Mo<sup>a,b</sup>, Xungai Wang<sup>c</sup>, Hongsheng Wang<sup>a,b,\*</sup>

<sup>a</sup> State Key Laboratory for Modification of Chemical Fibers and Polymer Materials, Donghua University, Shanghai 201620, P.R. China

<sup>b</sup> Biomaterials and Tissue Engineering Lab, College of Chemistry, Chemical Engineering and Biotechnology, Donghua University, Shanghai 201620, P.R. China

<sup>c</sup> Australian Future Fibres Research and Innovation Centre, Institute for Frontier Materials, Deakin University, VIC 3217, Australia

### ARTICLE INFO

#### Article history:

Received 5 September 2013

Received in revised form 6 December 2013

Accepted 16 December 2013

Available online 22 December 2013

#### Keywords:

Silk fibroin

Vitamin B<sub>5</sub>

Green electrospinning

Composite nanofiber

Biomedical application

Skin care product

### ABSTRACT

Silk fibroin (SF) from *Bombyx mori* has many established excellent properties and has found various applications in the biomedical field. However, some abilities or capacities of SF still need improving to meet the need for using practically. Indeed, diverse SF-based composite biomaterials have been developed. Here we report the feasibility of fabricating pantothenic acid (vitamin B<sub>5</sub>, VB<sub>5</sub>)-reinforcing SF nanofibrous matrices for biomedical applications through green electrospinning. Results demonstrated the successful loading of D-pantothenic acid hemicalcium salt (VB<sub>5</sub>-hs) into resulting composite nanofibers. The introduction of VB<sub>5</sub>-hs did not alter the smooth ribbon-like morphology and the silk I structure of SF, but significantly decreased the mean width of SF fibers. SF conformation transformed into β-sheet from random coil when composite nanofibrous matrices were exposed to 75% (v/v) ethanol vapor. Furthermore, nanofibers still remained good morphology after being soaked in water environment for five days. Interestingly, as-prepared composite nanofibrous matrices supported a higher level of cell viability, especially in a long culture period and significantly assisted skin cells to survive under oxidative stress compared with pure SF nanofibrous matrices. These findings provide a basis for further extending the application of SF in the biomedical field, especially in the personal skin-care field.

© 2013 Elsevier B.V. All rights reserved.

### 1. Introduction

Silk fibroin (SF) from domestic silkworm (*Bombyx mori*) cocoons is a natural biological protein polymer. It has many established excellent properties: good biocompatibility and biodegradability, tunable mechanical properties, controllable biodegradable rate *in vivo* and easily processing properties in aqueous environment [1–6]. Indeed, SF has received a great deal of attention from biomedical researchers since clinically used as surgical suture. It has been widely processed into particles, fibers, films, and gels for a variety of applications [2,4,7–9]. Recently, the research and application of SF nanofibers from electrospinning has become a hot topic in the biomedical field due to some unique properties of as-spun nanofibrous matrices. The specifically high surface-area-to-volume ratio and inherent porous structure of electrospun nanofibrous matrices closely mimics the natural extracellular matrix (ECM), making them very suitable for use as tissue regeneration and skin care

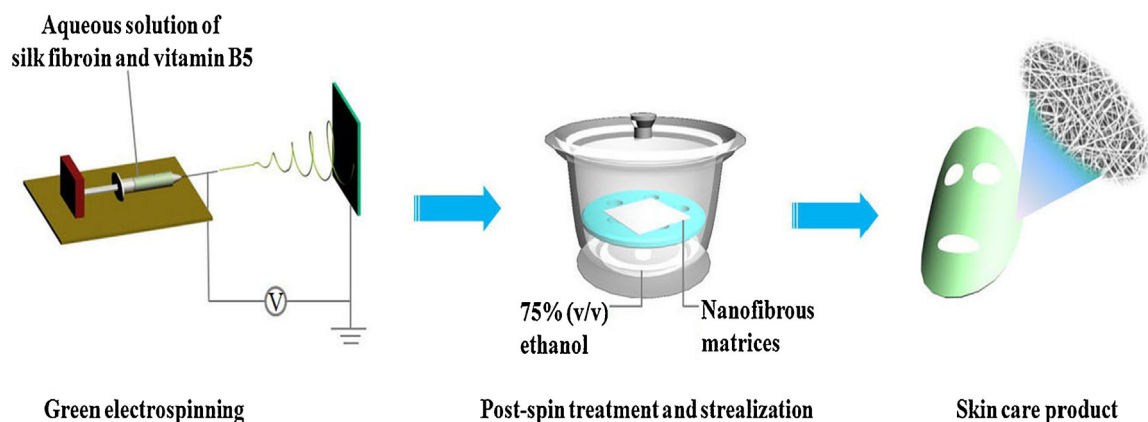
matrices [2,6,10–16]. However, some performances of electrospun SF nanofibrous matrices (ESFNM) such as antibacterial activity, bone-induced ability and antioxidation capacity still need further enhancing for special benefits. A good strategy is to develop SF-based hybrid or composite nanofibrous matrices with improved function [2,17,18].

Pantothenic acid, usually termed as vitamin B<sub>5</sub> (VB<sub>5</sub>), is an important component of coenzyme A. It plays a key role in numerous physiological responses and thus its deficiency often leads various diseases or disorders [19–21]. In particular, a wide range of studies have demonstrated the skin benefit of VB<sub>5</sub>. VB<sub>5</sub> can assist mammalian cells to survive in oxidative stress by increasing the level of glutathione, as revealed by Wojtczak et al. [22]. Aprahamian et al. reported that VB<sub>5</sub> supported fibroblast immigration and proliferation, and therefore promoted wound healing [23]. The clinical study from Leung et al. has also demonstrated that VB<sub>5</sub> can reduce sebum secretion, cure acne vulgaris and make smooth skin [24]. Therefore, VB<sub>5</sub> is a desired bioactive factor for personal skin care or tissue engineering products.

This work focuses on investigating the feasibility of fabricating VB<sub>5</sub>-reinforcing SF nanofibrous matrices via a green electrospinning process for biomedical applications (Scheme 1). The morphology of composite nanofibers was shown using SEM

\* Corresponding author at: College of Chemistry, Chemical Engineering and Biotechnology, Donghua University, 2999 North Renmin Road, Shanghai 201620, PR China. Tel.: +86 21 6779 2742; fax: +86 21 6779 2742.

E-mail addresses: [fanlinpeng2005@163.com](mailto:fanlinpeng2005@163.com), [whs@dhu.edu.cn](mailto:whs@dhu.edu.cn) (H. Wang).



**Scheme 1.** Green process of electrospinning pantothenic acid/silk fibroin composite nanofibers-based personal skin care products.

(scanning electron microscopy). The structure of nanofibrous matrices was analyzed by ATR-FTIR (attenuated total reflectance Fourier transform infrared spectroscopy). The loaded VB<sub>5</sub> within SF nanofibers was investigated using XPS (X-ray photoelectron spectroscopy). The cytocompatibility of VB<sub>5</sub>/SF nanofibrous matrices was shown through *in vitro* MTT (3-[4,5-dimethylthiazol-2-yl]-2,5-diphenyl tetrazolium bromide) viability assay and microscopic imaging of cells cultured on the composite fibrous matrices. The skin benefit of nanofibrous matrices was demonstrated through the viability of L929 cells grown on nanofibers under oxidative stress induced by *tert*-butyl hydroperoxide (*t*-BHP) *in vitro*.

## 2. Materials and methods

### 2.1. Materials

Cocoons from domestic silkworm (*B. mori*) were kindly provided by Jiaying Silk Company (China). D-Pantothenic acid hemicalcium salt: C<sub>9</sub>H<sub>16</sub>NO<sub>5</sub>·1/2Ca (VB<sub>5-hs</sub>) (purity ≥ 95.0%, HPLC) was purchased from Sigma–Aldrich (China). Mouse fibroblast L929 cells (L929 cells) were from the Institute of Biochemistry and Cell Biology (Chinese Academy of Sciences, China). All other reagents in this work were of analysis grade or higher. Ultrapure water used throughout this study was produced with a purification system (Rephile Shanghai Bioscience & Technology Co., Ltd., China) with a resistivity around 18 MΩ cm.

### 2.2. Preparation of regenerated silk fibroin (RSF)

RSF was fabricated as described in a previous study [2]. Briefly, cocoons were degummed in a boiling aqueous solution of 0.5% (w/v) Na<sub>2</sub>CO<sub>3</sub> three times (30 min each time) and then rinsed thoroughly with warm ultrapure water to remove the sericin. After being dried, degummed silk was dissolved in a ternary solvent system of CaCl<sub>2</sub>/H<sub>2</sub>O/CH<sub>3</sub>CH<sub>2</sub>OH solution (1:8:2 in molar ratio) at 65 °C. The resulting solution was dialyzed against ultrapure water with cellulose tube (molecular weight cutoff 14 kDa, Jing Ke Hong Da Biotechnology Co., Ltd., China) at ambient temperature for three days. Finally, RSF was obtained by lyophilizing the filtered SF solution.

### 2.3. Preparation of VB<sub>5-hs</sub>/SF composite nanofibrous matrices and post-spin treatment

VB<sub>5-hs</sub> powder and SF were respectively dissolved in ultrapure water. In this work, the amount of VB<sub>5-hs</sub> is 4 wt% based on the total

weight of VB<sub>5-hs</sub> and SF sponge. The VB<sub>5-hs</sub>/SF aqueous solution was obtained by adding SF solution into VB<sub>5-hs</sub> solution under uninterrupted agitation (the final concentration of SF solution is 30 wt%). The amount of VB<sub>5-hs</sub> was selected according to the previous report [25,26]. Then, the solution was filled into 2.5 mL plastic syringe capped with blunt needle. The syringe was located in syringe pump (Model 789100C, Cole-Parmer Instrument Co., USA) with a rate of 0.3 mL/h. A voltage of 20 kV generated with a high voltage power supply (BGG6-358, BMEICO, Ltd., China) was applied to the needle, a grounded aluminum foil as the collector and the distance between tip and collector was 20 cm. The electrospinning was performed at ambient temperature. After being dried, the resulting composite nanofibrous matrices were treated by placing them in a sealed desiccator saturated with 75% (v/v) ethanol vapor at ambient temperature [6].

### 2.4. Characterization

The morphology of nanofibers was observed with SEM (JEOLJSM-5600LV, Japan) after samples were sputter-coated with gold. The width distribution of as-spun fibers was determined using Image-J 1.34 software (National Institutes of Health, USA). At least 90 nanofibers from different SEM images for each sample were randomly measured.

To confirm the loading of VB<sub>5-hs</sub>, pure SF nanofibers and VB<sub>5-hs</sub>/SF composite nanofibers were respectively scanned using XPS (Escalab 250, Thermo Scientific Electron, East Grinstead, UK) with Mg K at 1486.6 eV and 150 W power at the anode, and the relative content of chemical elements was calculated from the peak height.

ATR-FTIR was carried out using an Avatar 380 FTIR instrument (Thermo Electron) in a wavenumber range of 1300–2000 cm<sup>-1</sup> and a resolution of 4 cm<sup>-1</sup>.

### 2.5. Cytocompatibility assessment

#### 2.5.1. Cell culture

L929 cells were incubated in a humidified incubator at 37 °C with 5% CO<sub>2</sub> using RPMI 1640 medium (Gibco) containing 10% fetal bovine serum (Gibco). Before cells seeded, pure and composite SF nanofibrous matrices were deposited on circular cover slips (14 mm in diameter). After being treated with 75% (v/v) ethanol vapor and dried in a sterilized fume hood, cover slips with nanofibrous matrices were directly placed into a 24-well cell culture plate without further sterilizing, and fixed with autoclaved stainless steel-rings. In this work, L929 cells were seeded at the density

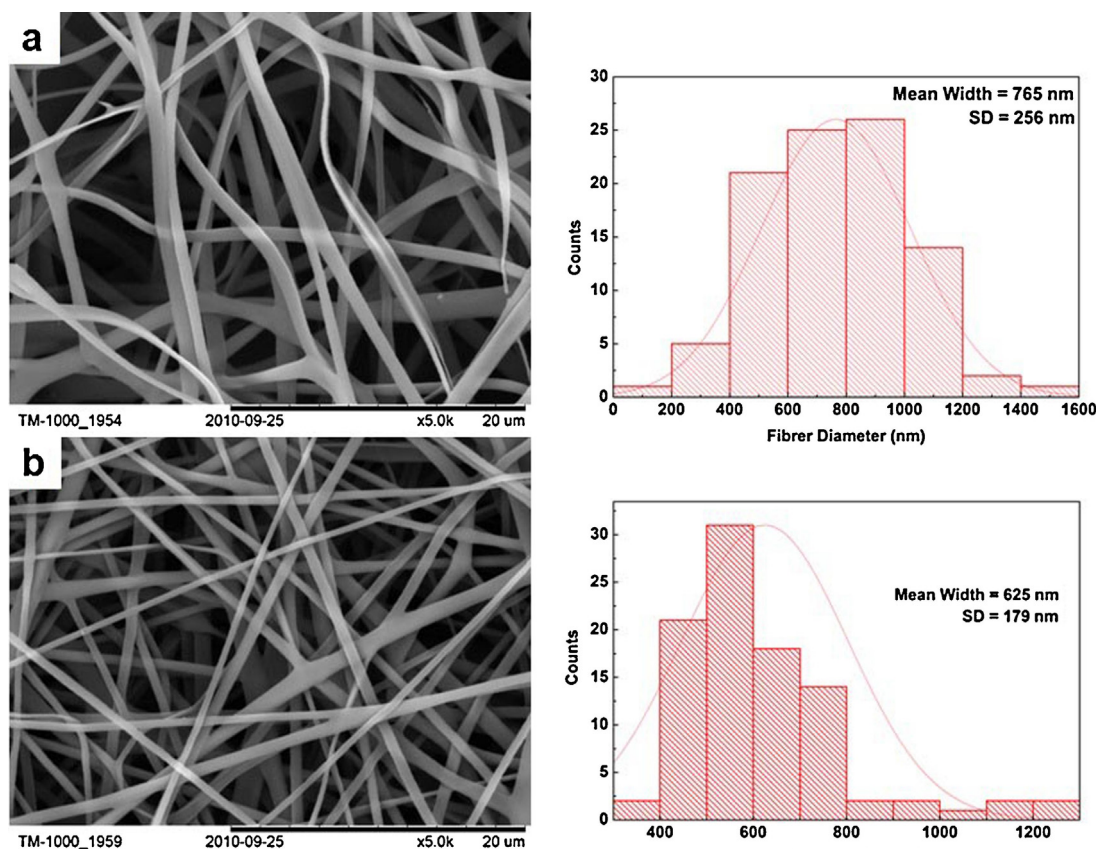


Fig. 1. SEM images of pure SF nanofibers (a) and VB<sub>5</sub>-hs/SF composite nanofibers (b).

of  $1.8 \times 10^4$  cells/well. For comparison, pure SF nanofibrous matrices were used as controls. The total volume of cells and medium was 400  $\mu$ L/each well when cells were seeded, and then each well was supplemented with 200  $\mu$ L of fresh medium every other day.

### 2.5.2. Cell viability assay

After cells cultured for one, three, five and seven days, the medium was removed and each well was rinsed with PBS (phosphate-buffered saline) three times. Then, 400  $\mu$ L of serum-free Dulbecco's modified Eagle's medium (DMEM) (Gibco) containing 0.5 mg/mL MTT (Sigma–Aldrich) was added to each well, followed by incubation for another 4 h. The formed formazan was dissolved in 400  $\mu$ L of dimethylsulfoxide and 100  $\mu$ L resulting solution of each sample was taken to determine the absorption at 492 nm using a microplate reader (Multiskan MK3; Thermo Lab-systems Co., China).

### 2.5.3. Cell morphology observation

The medium was removed on day three and 4% paraformaldehyde was used to fix the content for 20 min at 4 °C following rinsing each well with PBS. Then samples were respectively exposed to 30, 50, 70, 90, 95 and 100% (v/v) ethanol and dried in a sterilized fume hood. Subsequently, the samples were sputter-coated with gold and observed using SEM (JEOLJSM-5600LV, Japan).

### 2.6. Antioxidation assessment

Each well was rinsed with PBS three times following the medium removed on day four. Then, 400  $\mu$ L of serum-free DMEM containing different concentrations of *t*-BHP (60  $\mu$ M, 120  $\mu$ M and 240  $\mu$ M) was respectively added to the culture. Wells were rinsed three times

with PBS after *t*-BHP treatment for 24 h and the cell viability was determined using MTT assay as mentioned above.

### 2.7. Statistical analysis

All experiments were performed at least three times and data were reported as mean  $\pm$  standard deviation (SD). The error bars in the figures are the SD of the data. One-way ANOVA Statistical analysis was carried out on an Origin 7.5 (OriginLab, USA). In all statistical comparisons, a *p*-value of less than 0.05 was considered statistically significant. The data were indicated with (\*) for *p* < 0.05.

## 3. Results and discussion

### 3.1. Morphology of VB<sub>5</sub>/SF nanofibers

The surface morphology of VB<sub>5</sub>-hs/SF nanofibers was revealed using SEM (Fig. 1). Clearly, the incorporation of VB<sub>5</sub>-hs did not significantly alter the ribbon-like and smooth morphology of SF nanofibers. The smaller width of composite nanofibers (625  $\pm$  179 nm) than that of pure SF nanofibers (765  $\pm$  256 nm) is probably due to the increased solution conductivity with VB<sub>5</sub>-hs species in the electrospinning solution [27]. Both pure and VB<sub>5</sub>-hs-loaded SF nanofibers became compact and cross-linked each other after being treated via 75% (v/v) ethanol vapor (Fig. 2a and b). This is presumably caused by two reasons: firstly, nanofibers were further dehydrated in 75% (v/v) ethanol vapor environment; secondly, the presence of 75% (v/v) ethanol vapor induced SF structure transition from silk I into silk II [6]. The good morphology of the treated nanofibers exposed to water environment for five days indicates their excellent water-resistant ability (Fig. 2a' and b').

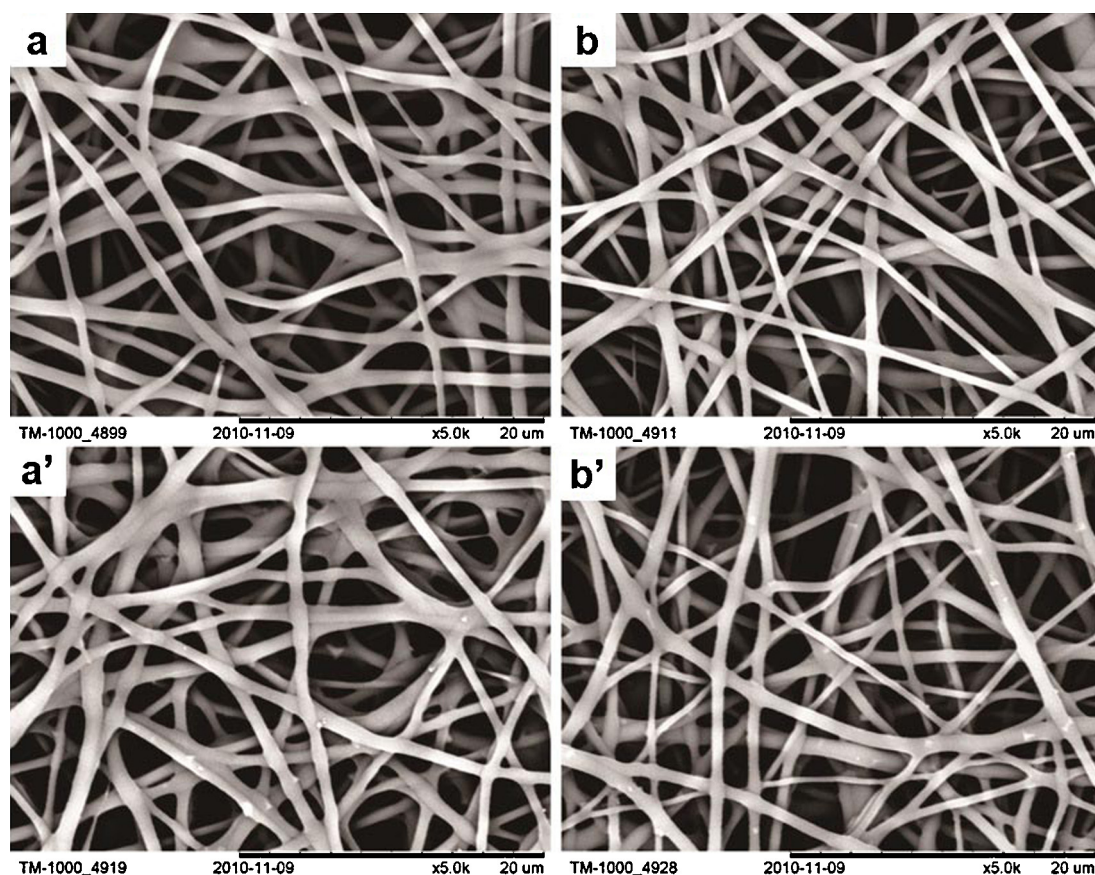


**Fig. 2.** SEM images of nanofibers with 75% (v/v) ethanol vapor treatment ((a) pure SF nanofibers and (b) VB<sub>5-hs</sub>/SF composite nanofibers) and nanofibers exposed to water environment for five days after treatment with 75% (v/v) ethanol vapor ((a') pure SF nanofibers and (b') VB<sub>5-hs</sub>/SF composite nanofibers).

### 3.2. Loading of VB<sub>5-hs</sub> into SF nanofibers

The loading of VB<sub>5-hs</sub> in SF nanofibers was confirmed by XPS spectroscopy (Fig. 3) and the relative content of chemical elements from the post-treated nanofibers is listed in Table S1 (Supporting information). Although C, O and N peaks were observed in

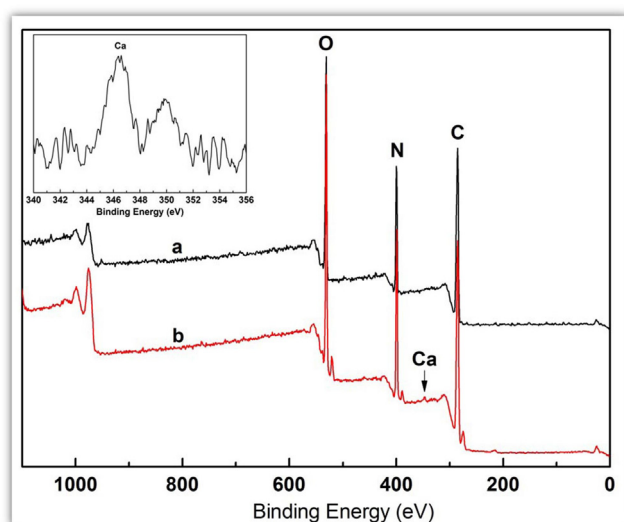


**Fig. 3.** XPS spectra of pure SF nanofibers (a) and VB<sub>5-hs</sub>/SF composite nanofibers (b) (the inset is a magnification of Ca peak).

the XPS spectra of both samples, the characteristic peak of Ca only emerged in the spectrum of composite nanofibers (Fig. 3b). Clearly, the presented Ca of 0.29% demonstrates the successful loading of VB<sub>5-hs</sub> into SF nanofibers according to the elemental composition of VB<sub>5-hs</sub> and SF (Table S1, Supporting information).

Supplementary material related to this article can be found, in the online version, at <http://dx.doi.org/10.1016/j.colsurfb.2013.12.030>.

### 3.3. Structure of composite nanofibrous matrices

The structure of SF from different samples (pure SF nanofibers, composite nanofibers and composite nanofibers with 75% (v/v) ethanol vapor treatment) was identified using ATR-FTIR spectroscopy (Fig. 4). The characteristic absorption bands of SF (1700–1600 cm<sup>-1</sup> for amide I and 1600–1500 cm<sup>-1</sup> for amide II) from pure SF nanofibers at 1651 cm<sup>-1</sup> and 1536 cm<sup>-1</sup> are attributed to silk I SF (in which random coil conformation prevails) (Fig. 4a) [18]. SF of composite nanofibers also showed the characteristics of silk I structure, presenting characteristic absorption peaks similar to those of pure SF nanofibers (Fig. 4b). However, SF from composite nanofibers exhibited a shift in peak positions from 1648 cm<sup>-1</sup> and 1538 cm<sup>-1</sup> to 1626 cm<sup>-1</sup> and 1517 cm<sup>-1</sup> after the nanofibers treated with 75% (v/v) ethanol vapor (Fig. 4b and d), which is similar to that of treated pure SF nanofibers (Fig. 4a and c). The presence of new peaks (1699 cm<sup>-1</sup> for treated pure SF nanofibers and 1700 cm<sup>-1</sup> for treated composite SF nanofibers) and the shift in peak positions above suggest silk II SF (in which β-sheet conformation is dominant). Therefore, the introduction of VB<sub>5-hs</sub> did not

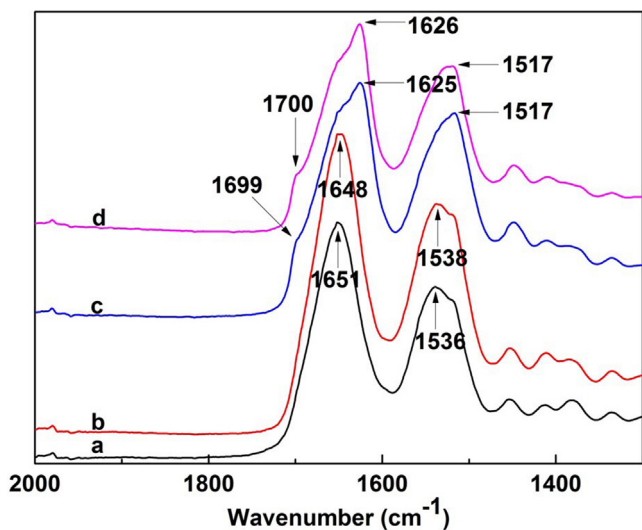


**Fig. 4.** ATR-FTIR spectra of nanofibers before post-spin treatment ((a) pure SF nanofibers and (b) VB<sub>5-hs</sub>/SF composite nanofibers) and nanofibers with 75% (v/v) ethanol vapor treatment ((c) pure SF nanofibers and (d) VB<sub>5-hs</sub>/SF composite nanofibers).

produce significant change in SF structure and the treatment of 75% (v/v) ethanol vapor induced SF structure from silk I (a water-unstable structure) into silk II (a water-stable structure). This is consistent with the excellent water-resistant property of post-treated nanofibers (Fig. 2a' and b').

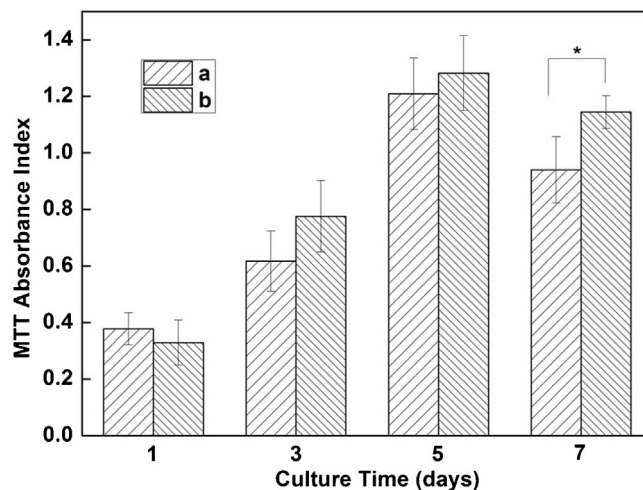


**Fig. 5.** The viability of L929 cells grown on nanofibers ((a) pure SF nanofibers and (b) VB<sub>5-hs</sub>/SF composite nanofibers). Data are reported as mean  $\pm$  standard deviation (SD) and error bars represent SD ( $n = 4$ ). \* $p < 0.05$ .

### 3.4. Cytocompatibility assay

The excellent cytocompatibility of ESFNM have been demonstrated in the previous study [6]. Therefore, ESFNM is used as a control to examine the applicability of VB<sub>5-hs</sub>/SF nanofibers for skin care and tissue engineering in this work. The proliferation viability of L929 cells on nanofibrous matrices was revealed using MTT assay (Fig. 5). Within the first five days of the culture period, the cell population on both ESFNM and VB<sub>5-hs</sub>/ESFNM continuously

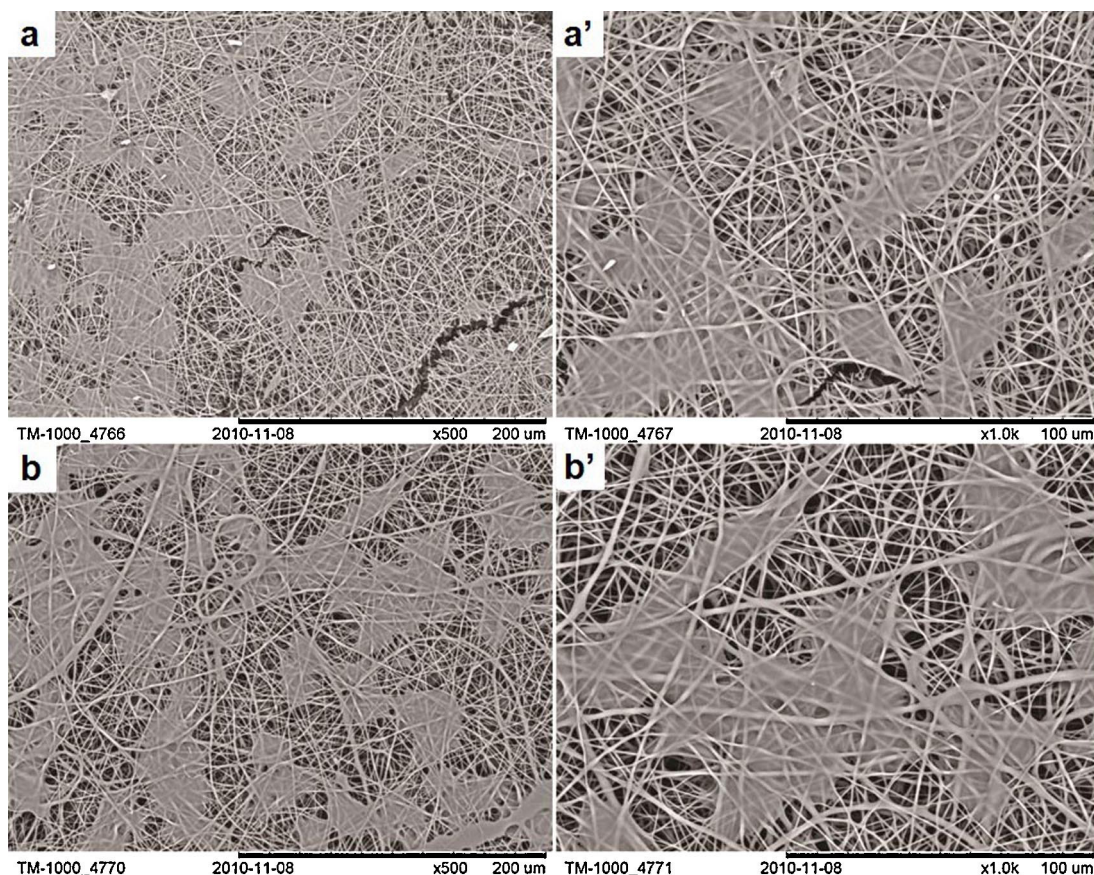


**Fig. 6.** The morphology of L929 cells grown on nanofibers: pure SF nanofibers at 500 $\times$  (a) and 1000 $\times$  (a'); VB<sub>5-hs</sub>/SF composite nanofibers 500 $\times$  (b) and 1000 $\times$  (b').

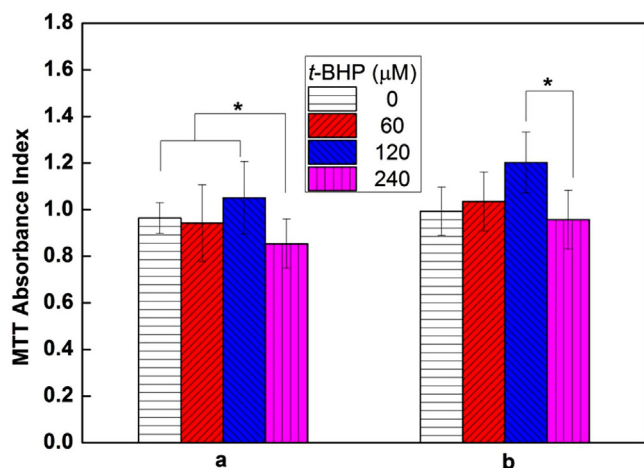


**Fig. 7.** The viability of L929 cells grown on nanofibers under oxidative stress induced by different concentrations of *t*-BHP ((a) pure SF nanofibers and (b) VB<sub>5-hs</sub>/SF composite nanofibers). Data are reported as mean  $\pm$  standard deviation (SD) and error bars represent SD ( $n = 4$ ). \* $p < 0.05$ .

increased with an extended time and no observed significant difference between them. However, on the day seven, both types of nanofibrous matrices produced a significant decrease in the cell population compared with day five. Presumably, fast cell proliferation led to a deteriorated environment including nutrient deficiency and metabolic accumulation, and in turn inhibited cell viability and population. In this case, the presence VB<sub>5-hs</sub> could assist L929 cells to survive, therefore suggesting a higher level of cell viability on composite nanofibrous matrices. The mechanism underlining this needs to be further understood.

To further reveal the cell–cell and cell–matrix interaction, the morphology of L929 cells cultured on nanofibrous matrices for three days was scanned using SEM (Fig. 6). L929 cells proliferated and spread very well on both ESFNM and VB<sub>5-hs</sub>/ESFNM. Clearly, cells mainly adopted a typical fusiform shape and bridged each other on nanofibers.

### 3.5. Protection by nanofibrous matrices against oxidative insult induced by *t*-BHP

The previous study has demonstrated the protection of VB<sub>5</sub> or its derivatives to various types of cells against oxidative stress [22,28,29]. In this work, the biological activity of composite nanofibrous matrices was further examined by an oxidative injury model: L929 cells cultured on nanofibrous matrices for five days were challenged by oxidative insult induced by *t*-BHP (a model compound for inducing reactive oxygen species (ROS) or oxidative stress [30]) (Fig. 7). Indeed, ROS regulates the redox (reduction/oxidation) balance in cells or tissues by working as negative or positive messengers in signal-transduction pathways. The disruption of the balance alters cellular functions. Therefore, overwhelming amount of ROS leads to cell death or the development of diseases, whereas moderate levels of ROS could increase cell viability and survival [31–33]. In the concentration range of 0–120  $\mu$ M, the addition of *t*-BHP did not decrease the viability of L929 cells on both pure and composite SF nanofibrous matrices. On the contrary, there seems to present an increasing trend in the cell viability. With further increasing the concentration of *t*-BHP to 240  $\mu$ M, the cell viability of pure SF nanofibrous matrices significantly reduced compared with the control without *t*-BHP. However, there existed no obvious difference for the composite nanofibrous group. This suggests the incorporation of VB<sub>5-hs</sub> significantly assisted L929 cells grown on SF nanofibrous matrices to survive under oxidative stress. The significant difference in the cell viability between 120  $\mu$ M and 240  $\mu$ M

of *t*-BHP for two types of fibers could be due to the disruption of redox balance in L929 cells.

## 4. Conclusion

In this work, we successfully fabricated pantothenic-acid-loaded silk fibroin composite nanofibrous matrices using a green electrospinning technique. As-spun composite nanofibrous matrices maintained a higher level of cell viability, especially in a long culture period and significantly assisted skin cells to survive under oxidative stress compared with pure silk fibroin nanofibrous matrices. The ongoing progress in our lab is to achieve pantothenic acid/silk fibroin composite nanofibers with the desired release behaviors of pantothenic acid for practical applications based on the tunable properties of silk fibroin. The present work provides a basis for further extending the application of silk fibroin in the biomedical field, especially in personal skin-care field.

## Acknowledgements

This research was supported by the Shanghai–Unilever Research and Development Fund (08520750100), the Natural Science Foundation of Shanghai (12ZR1400300), National Nature Science Foundation of China (31070871 and 31271028), Fundamental Research Funds for the Central Universities and Open Foundation of State Key Laboratory for Modification of Chemical Fibers and Polymer Materials (LK1111).

## References

- [1] B.M. Min, G. Lee, S.H. Kim, Y.S. Nam, T.S. Lee, W.H. Park, *Biomaterials* 25 (2004) 1289–1297.
- [2] L.P. Fan, H.S. Wang, K.H. Zhang, Z.X. Cai, C.L. He, X.Y. Sheng, X.M. Mo, *RSC Adv.* 2 (2012) 4110–4119.
- [3] R.L. Horan, K. Antle, A.L. Collette, Y.Z. Wang, J. Huang, J.E. Moreau, V. Volloch, D.L. Kaplan, G.H. Altman, *Biomaterials* 26 (2005) 3385–3393.
- [4] G.H. Altman, F. Diaz, C. Jakuba, T. Calabro, R.L. Horan, J.S. Chen, H. Lu, J. Richmond, D.L. Kaplan, *Biomaterials* 24 (2003) 401–416.
- [5] J. Zhou, C.B. Cao, X.L. Ma, L. Hu, L. Chen, C.R. Wang, *Polym. Degrad. Stabil.* 95 (2010) 1679–1685.
- [6] L.P. Fan, H.S. Wang, K.H. Zhang, C.L. He, Z.X. Cai, X.M. Mo, *J. Biomater. Sci. Polym. E* 23 (2012) 497–508.
- [7] A.S. Lammel, X. Hu, S.H. Park, D.L. Kaplan, T.R. Scheibel, *Biomaterials* 31 (2010) 4583–4591.
- [8] U.J. Kim, J. Park, C.M. Li, H.J. Jin, R. Valluzzi, D.L. Kaplan, *Biomacromolecules* 5 (2004) 786–792.
- [9] N. Minoura, M. Tsukada, M. Nagura, *Biomaterials* 11 (1990) 430–434.
- [10] K.H. Kim, L. Jeong, H.N. Park, S.Y. Shin, W.H. Park, S.C. Lee, T.I. Kim, Y.J. Park, Y.J. Seol, Y.M. Lee, Y. Ku, I.C. Rhyu, S.B. Han, C.P. Chung, *J. Biotechnol.* 120 (2005) 327–339.
- [11] C. Huang, R. Chen, Q.F. Ke, Y. Morsi, K.H. Zhang, X.M. Mo, *Colloids Surf. B: Biointerfaces* 82 (2011) 307–315.
- [12] C. Huang, Y.W. Tang, X. Liu, A. Sutti, Q.F. Ke, X.M. Mo, X.G. Wang, Y. Morsi, T. Lin, *Soft Matter* 7 (2011) 10812–10817.
- [13] H.F. Guo, Z.S. Li, S.W. Dong, W.J. Chen, L. Deng, Y.F. Wang, D.J. Ying, *Colloids Surf. B: Biointerfaces* 96 (2012) 29–36.
- [14] X.Q. Li, Y. Su, S.P. Liu, L.J. Tan, X.M. Mo, S. Ramakrishna, *Colloids Surf. B: Biointerfaces* 75 (2010) 418–424.
- [15] K.H. Zhang, L.P. Fan, Z.Y. Yan, Q.Z. Yu, X.M. Mo, *J. Biomater. Sci. Polym. E* 23 (2012) 1185–1198.
- [16] L.P. Fan, Z.X. Cai, C.C. Wu, X.H. Geng, H.S. Wang, C.L. He, X.M. Mo, *Adv. Mater. Res.* 160–162 (2011) 1165–1169.
- [17] Z.X. Cai, X.M. Mo, K.H. Zhang, L.P. Fan, A.L. Yin, C.L. He, H.S. Wang, *Int. J. Mol. Sci.* 11 (2010) 3529–3539.
- [18] C.M. Li, C. Vepari, H.J. Jin, H.J. Kim, D.L. Kaplan, *Biomaterials* 27 (2006) 3115–3124.
- [19] R.E. Olson, N.O. Kaplan, *J. Biol. Chem.* 175 (1948) 515–530.
- [20] J.J. Ellestad-Sayed, R.A. Nelson, M.A. Adson, W.M. Palmer, E.H. Soule, *Am. J. Clin. Nutr.* 29 (1976) 1333–1338.
- [21] A.E. Axelrod, *Am. J. Clin. Nutr.* 24 (1971) 265–271.
- [22] L. Wojtczak, V.S. Slyschenkov, *Biofactors* 17 (2003) 61–73.
- [23] M. Aprahamian, A. Dentinger, C. Stock-Damge, J.C. Kouassi, J.F. Grenier, *Am. J. Clin. Nutr.* 41 (1985) 578–589.
- [24] L.H. Leung, *Med. Hypotheses* 44 (1995) 490–492.
- [25] Z.D. Draeos, *Curr. Probl. Dermatol.* 12 (2000) 235–239.
- [26] E. Nicolaidou, A.D. Katsambas, *Clin. Dermatol.* 18 (2000) 87–94.

- [27] H. Cao, X. Chen, L. Huang, Z.Z. Shao, *Mater. Sci. Eng. C* 29 (2009) 2270–2274.
- [28] V.S. Slyshenkov, K. Piwocka, E. Sikora, L. Wojtczak, *Free Radical Biol. Med.* 30 (2001) 1303–1310.
- [29] B. Etensel, S. Özkisacik, E. Özkara, A. Karul, O. Öztan, M. Yazici, H. Gürsoy, *Pediatr. Surg. Int.* 23 (2007) 177–181.
- [30] S.J. Bae, J.S. Lee, J.M. Kim, E.K. Lee, Y.K. Han, H.J. Kim, J. Choi, Y.M. Ha, J.K. No, Y.H. Kim, B.P. Yu, H.Y. Chung, *J. Agric. Food Chem.* 58 (2010) 6387–6394.
- [31] D. Trachootham, W.Q. Lu, M.A. Ogasawara, N.R.D. Valle, P. Huang, *Antioxid. Redox Signal.* 10 (2008) 1343–1374.
- [32] H.C. Lee, P.H. Yin, C.W. Chi, Y.H. Wei, J. Biomed. Sci. 9 (2002) 517–526.
- [33] M. Yoneyama, K. Kawada, Y. Gotoh, T. Shiba, K. Ogita, *Neurochem. Int.* 56 (2010) 740–746.